Supporting Information for "Quantitative time-course metabolomics in human red blood cells reveal the temperature dependence of human metabolic networks"

JT Yurkovich et al.

Contents

List of Figures

RBC unit preparation and data measurement. Whole blood was collected from three healthy blood donors into 63 mL of CPD anticoagulant solution (Fenwall, Lake Zurich, IL, USA) and was held on butanediol plates for minimum of 2 hours at 4°C. After separation of plasma and buffy coat by centrifugation (800g, 11 minutes, 20°C), RBCs were suspended in 100 mL of SAGM additive solution (Fenwal) and leukodepleted using a SEPACELL Pure RC white cell reduction filter (Asahi Corporation, Tokyo, Japan). Each unit was split into 4 standard Pediatric storage containers (Fenwall) and samples were collected via sterile connected clave valve collected into a syringe with a Luer-Lock connector on different time points. The National Bioethics Committee of Iceland and Icelandic Data Protection Authority approved the study.

RBC samples were first processed to separate supernatant and cells by centrifugation of 0.5 mL of RBC (1600g, 15 min, 4°C) and then prepared separately. Immediately after centrifugation, cell-free supernatant was removed and collected in separate tubes. RBC supernatant (80 μL) was processed by adding internal standard mixture (30 μL) and methanol (0.5 mL). The internal standard mixture contained the following standards: phenylalanine d2 (72 mg/L), succinate d4 (50 mg/L), glucose 13C6 (2100 mg/L), carnitine d9 (20 mg/L), glutamic acid d5 (30 mg/L), lysine d4 (90 mg/L). Alanine d4 (300 mg/L), AMP 13C1015N5 (50 mg/L) and 1 mL of -20°C methanol-water (7:3) were added to the cell pellets. Cells were lysed by two freeze and thaw steps. Samples were centrifuged (15000g, 20 min, 4°C) and supernatant was transferred into a new tube. 1 mL of 20°C methanol-water (7:3) (1 mL) was added to pellets and samples were vortexed for 1 min, centrifuged (15000g, 20 min, 4°C) and supernatant was added to the precedent. Samples were dried using a vacuum concentrator, reconstituted in 300 μL H_2O:ACN (50:50), and filtered to remove residual hemoglobin by centrifugation (Amicon Ultra 0.5 mLfilter, 15000g, 4°C, 60 min). The first sample was taken one day after storage had begun; this time point is taken as $t = 0$ in all figures.

At each time point, we monitored typical QC/QA hematological parameters of RBC physiology. A blood gas analyzer (ABL90FLEX, Radiometer, Copenhagen Denmark) was used to determine pH (37°C), pO2, and pCO2, total hemoglobin, K+, Na+, Cl- in the media. RBC concentration, mean RBC volume, hematocrit, RBC distribution width, and white blood cell count were assayed using an hematoanlyzer (CELLDYN Ruby, Abbot Diagnostics, Lake Forest, IL, USA). Hemolysis was calculated using the following formula: % hemolysis = (supernatant Hb (g/L)/total Hb (g/L)) × (100-Hct (%)), where total Hemoglobin (Hb) and hematocrit was analyzed using a hematoanalyzer and supernatant Hb was measured with a HemoCue Plasma/Low Hb system (HemoCue, Angelshol, Sweden). Adenosine triphosphate (ATP) and 2,3-diphosphoglycerate (2,3-DPG) concentrations, employing the CellTiter-Glo kit (Promega) and the 2,3-DPG kit (Roche Diagnostics), respectively. Lactate dehydrogenase (LDH) activity was assessed by an LDH assay kit (ab102526, Abcam, Cambridge, UK).

Bacterial testing was performed at the end of the study. 10 mL from each unit was injected into a BacT/Alert FA Plus flasks for aerobic bacteria and BacT/Alert FN Plus flasks for anaerobic bacteria. The flasks were cultured for 5 days on a BacT/ALERT 3D microbial detection system (BioMérieux, Marcy l'Etoile, France) and analyzed by a specialist in medical microbiology.

QC/QA measurements. The measured hemolysis was almost identical at 4°C and 13°C within the accepted range (<0.8% cells), while the threshold was exceeded at 22°C and 37°C as the storage time progressed. The activity of lactate dehydrogenase and the concentration of free hemoglobin closely matched this trend. The pH fell from approximately 7 at all temperatures to around 6.4 before rising. The average mass of hemoglobin per cell was calculated and, although noisy, was approximately the same across all temperatures.

Glycolysis and pentose phosphate pathway. In glycolysis and the pentose phosphate pathway (PPP), glucose (both intracellular and extracellular), intracellular oxidized glutathione, 6-phosphogluconate, glucose 6-phosphate, fructose 1,6-bisphosphate (FBP), the phosphoglycerate pool, and phosphoenolpyruvate were all observed to deplete, while lactate (both intracellular and extracellular) accumulated at a rate that increased consistently with temperature. The temperature vs. rate plots for glucose and glutathione displayed similar qualitative behavior with slightly nonlinear shapes, while fructose 1,6-bisphosphate, lactate, glucose 6-phosphate, and phosphoenolpyruvate all displayed highly linear behavior.

Several key metabolites from the nucleotide synthesis and salvage pathways were measured. There was an accumulation of intracellular xanthine which drastically increased with temperature, leading to one of the highest Q_{10} values found (4.84). There was also an accumulation of hypoxanthine (both intracellular and extracellular), extracellular xanthine, and uridine (both intracellular and extracellular). Intracellular GMP and IMP both depleted, with the latter showing an initial spike that increased in magnitude with increasing temperature. The behavior displayed by extracellular uridine at 37°C was the most noticeable here as there is no corresponding jump at 22°C. Three of these measurements—GMP, intracellular hypoxanthine, and extracellular hypoxanthine—had Q_{10} values of approximately 1.5, while the other measurements (with the exception of xanthine) had values that were all approximately 3.

The partial pressure of carbon dioxide rose initially but fell drastically at 13°C, 22°C, and 37°C, leading to a nonlinear shape and reduced R2 value in the temperature vs. rate plot. 6-phosphogluconate, the phosphoglycerate pool, phosphoenolpyruvate, and glucose 6-phosphate all had Q_{10} values around 3, while the majority of the other measurements had values closer to 2. Some metabolites in adjacent reactions, like the phosphoglycerate pool and phosphoenolpyruvate, had very similar Q_{10} values, while others (e.g., intracellular vs. extracellular lactate) had different Q_{10} values. 2,3-Disphosphoglycerate (2,3-DPG) has previously been implicated in RBC storage lesion (1). While we did not measure 2,3-DPG, the similar trends observed in intracellular S-Adenosylmethioninamine (SAM), hypoxanthine, and intracellular oxidized glutathione to previous measurements (2) indicate that the 2,3-DPG trend is also consistent.

Glutathione synthesis. In the glutathione synthesis pathway, there was an accumulation of 5-oxoproline (both intracellular and extracellular), extracellular glutamate, and extracellular

serine (Figure S2). We observed a depletion of both intracellular and extracellular reduced glutathione depleted, except for the extracellular at 37°C increased after an initial depletion; no later increase in concentration was reported at 4°C for extracellular reduced glutathione through 42 days of storage (2). Intracellular oxidized glutathione depleted with increased temperature, while the extracellular measurement displayed a large spike at 22°C and 37°C that was not observed at low temperatures; this spike was not observed through 42 days of storage at 4°C (2). Extracellular glutamine showed large initial spikes in concentration at 22°C and 37°C that were not observed at low temperatures through 21 days.

Amino acid metabolism. We measured 15 amino acids. Many of these measurements were considered too noisy to be included in the Q_{10} calculations, although general qualitative trends were still visible. We observed increasing concentrations of extracellular L-glutamate, intracellular and extracellular L-lysine, intracellular and extracellular L-phenylalanine, extracellular L-serine, and intracellular L-tryptophan.

At high temperatures, both intracellular and extracellular L-histidine increased while concentrations remained fairly steady at low temperatures. The same behavior was observed for the intracellular and extracellular L-isoleucine/L-leucine pools. Several concentrations remained rather steady, including intracellular L-arginine, intracellular L-asparagine, intracellular L-aspartate, and intracellular L-threonine. Intracellular L-glutamate decreased steadily at 4°C and 13°C but later increased at high temperatures. Intracellular and extracellular L-glutamine both showed an initial spike followed by a depletion. The depletion was more pronounced at high temperatures. The measurements for intracellular L-serine, L-arginine, L-asparagine, the L-isoleucine/L-leucine pool, L-histidine, L-phenylalanine, L-threonine, L-tryptophan, L-tyrosine, and L-valine as well as the extracellular L-isoleucine/L-leucine pool were too noisy to determine meaningful trends.

Ion profiles. One of the more interesting results was the behavior of the measured ions: extracellular chloride, potassium, and sodium (Figure S3). The trends observed in potassium and sodium at 4°C and 13°C were similar, with small quantitative differences. At 22°C and 37°C, the same changes were observed to be more pronounced. It can be expected that the magnitude of change in potassium concentration is greater than that of sodium (3), a behavior which was observed here across all temperatures. Sodium was among the slowest-scaled measurements ($Q_{10} = 1.63$), while chloride and potassium were closer to the center of the distribution ($Q_{10} = 2.44$ and $Q_{10} = 2.14$, respectively).

At low temperatures, the membrane ATPase in RBCs undergoes a reversible inhibition which shuts down active Na/K transport and instead allows for a steady leak of cations across the membrane (3, 4). Consequently, extracellular potassium is expected to rise and extracellular sodium is expected to fall at low temperatures since the Na/K pump is not actively pumping ions back across the membrane. At high temperatures when the pump is functioning properly, we can expect to observe steady cation concentrations. However, our results here do not coincide with these expectations, as we see the same fall of sodium levels and rise of potassium levels at all temperatures (Figure S3). One contributing factor to these results is the depletion of intracellular ATP (2), which is required for the Na/K pump to function. As ATP depletes, the Na/K pump will function slower, resulting in a rise in extracellular potassium and fall of extracellular sodium as observed here. Another possible explanation for the unexpected cation behavior involves the role of magnesium in membrane ATPase activity. It has been previously suggested that the citrate additive meant as an anticoagulant could bind free magnesium ions, further inhibiting ATPase activity (3). We observed increasing amounts of intracellular citrate at 22°C and 37°C but steady, low concentrations at 4°C and 13°C. Thus, if the large amounts of intracellular citrate are bound to magnesium at high temperatures, the irregular behavior of citrate and the cations could be related. Ultimately, the implications of the cation behavior seen here are uncertain and require further investigation.

Measurements with qualitatively different behavior across temperature. A few measurements exhibited qualitatively different concentration profiles across the four temperatures. The most drastic difference was observed in extracellular oxidized glutathione (Figure S3). Using the initial slope to fit this nonlinear profile allowed us to account for the magnitude of the spike observed at higher temperatures; this resulted in a calculated Q_{10} value of 6.75, the highest among all measurements. Intracellular citrate showed a similar concentration spike at high temperatures that was not observed at low temperatures (Figure S3). Previous studies reported a decreasing concentration of citrate at 4°C over 42 days of storage in SAGM, with a slight spike just before day 40 (2), which matches the trend observed here at 4°C. Intracellular inosine exhibited no clear trend across temperature, with a substantial spike at 37°C that is not present at the other three temperatures (Figure S3). Even at 37°C, however, the concentration of inosine was very low most likely due to its toxicity (5).

Mechanistic basis for Temperature Dependence. Above, we provided an observational characterization of the data. Here, we attempt to provide a mechanistic explanation for the Q_{10} values that were calculated (i.e., why are some high and some low?). We explored three rationale based on (1) network location, (2) metabolite properties, and (3) enzymatic thermostability.

First, we checked for systems-level spatial trends within the calculated Q_{10} values. A "spatial trend" (i.e., distance within the network) would be observed if metabolites adjacent to one another in metabolic pathways shared similar Q_{10} values. We calculated the distance (defined as the number of reaction steps apart) between all measured metabolites in the network pairwise, but no spatial trend was observed. This result indicates that network proximity does not influence the Q_{10} values of the measured metabolites.

In order to explore any spatial trends among Q_{10} values, we computed the distance between every measured metabolite pairwise using the network model. Distance is defined as the number of reaction steps that separate two metabolites. For this calculation, we excluded all highly-connected metabolites: intracellular ADP, L-glutamate, sodium and extracellular ATP and sodium.

Next, we hypothesized that certain metabolite properties might influence the calculated Q_{10} values. In particular, we investigated metabolite properties related to diffusive capacity: volume, mass, partition coefficient (LogP), and water accessible

surface area. Again, we observed no correlation between Q_{10} values and these metabolite properties. Although far from comprehensive, the analysis here indicates that metabolite properties and the diffusive capacity of individual metabolites also has no influence a metabolite's Q_{10} value.

Calculator Plugins were used for the calculation of all metabolite properties, provided by Marvin 15.11.16.0, 2015, from ChemAxon (http://www.chemaxon.com). The Chemical Entities of Biological Interest (ChEBI) identifier was obtained for each metabolite and converted into an InChI string for input to the ChemAxon command-line binary for calculation.

Finally, we explored whether the thermostability of enzymes were related to Q_{10} values. We calculated the thermostability of every enzyme in the metabolic network reconstruction that interacted with one of the measured metabolites, plotting the max velocity of each enzyme as a function of temperature (6). We once again observed no correlation between the optimal temperature of enzymes and the Q_{10} values of the corresponding metabolites.

We followed the workflow from Chang et al. (6) in order to calculate the temperature-dependent protein activity for all enzymes that interact with measured metabolites. This allowed us to plot the velocity of an enzyme as a function of temperature. The peak of this plot represents the temperature of maximal protein activity (T_o). For each enzyme, this value was correlated with the Q_{10} value for metabolites that interacted with the enzyme.

While these efforts certainly do not represent an exhaustive search, they did not provide any meaningful explanation for a mechanistic basis for the calculated Q_{10} values.

Integration with metabolic network reconstruction. We used a version of the cell-scale metabolic network reconstruction of the human erythrocyte iAB-RBC-283 (7) that had been modified for use in building personalized kinetic models (8). In order to perform flux modeling, we estimated the concentration profile of 2,3-DPG according to (9). The flux coupling of reactions was calculated using F2C2 (10). In the main text, we defined the coupling characteristic of a network to be the mean of the length of coupled reaction sets; this mean was calculated from the distribution of the length of the reaction sets at each temperature (Figure S4). Only fully-coupled reactions were considered for this analysis (i.e., partially-coupled and directionally-coupled reactions were excluded). Coupled reactions that shared nodes were then combined in order to form coupled reaction sets.

Table S1. Quantitative analysis for selected intracellular metabolites (endometabolomics measurements).

HMDB ID	Metabolite	Linear range (mg/L)	Slope ± STD	Intercept ± STD	r ± STD	LLOD (mg/L)
HMDB00687/HMDB0000172	(Iso)leucine	3.75-60	0.06 ± 0.01	-0.16 ± 0.05	0.990 ± 0.006	1.4
HMDB01173	5-MTA	0.156-2.5	9.46 ± 2.59	10.58 ± 4.23	0.995 ± 0.003	0.05
HMDB00267	5-oxoproline	10-160	0.45 ± 0.14	1.42 ± 0.29	0.995 ± 0.003	1.9
HMDB01316	6-phosphogluconate	3.75-60	0.04 ± 0.01	-0.18 ± 0.03	0.994 ± 0.001	0.3
HMDB00201	Acetylcarnitine	0.12-2	1.11 ± 0.21	0.17 ± 0.05	0.997 ± 0.004	0.08
HMDB00958	Aconitate	1.25-20	1.27 ± 0.06	0.32 ± 0.16	0.994 ± 0.006	0.4
HMDB00034	Adenine	5-80	1.99 ± 0.29	-1.59 ± 0.42	0.995 ± 0.002	0.04
HMDB01539	ADMA	1.25-10	2.52 ± 0.31	5.02 ± 0.53	0.989 ± 0.003	0.3
HMDB01341	ADP	37.5-600	0.04 ± 0.01	-1.46 ± 0.47	0.996 ± 0.003	0.6
HMDB00045	AMP	37.5-600	0.11 ± 0.01	-2.06 ± 0.06	0.999 ± 0.0003	0.3
HMDB00517	Arginine	1.25-20	0.84 ± 0.06	0.07 ± 0.04	0.994 ± 0.004	0.2
HMDB00168	Asparagine	3.75-60	0.28 ± 0.05	-0.99 ± 0.21	0.994 ± 0.004	0.5
HMDB00191	Aspartate	6.25-100	0.25 ± 0.05	0.75 ± 0.36	0.996 ± 0.003	1.1
HMDB00062	Carnitine	0.12-2	1.09 ± 0.06	-0.11 ± 0.04	0.997 ± 0.001	0.06
HMDB00097	Choline	0.312-5	0.50 ± 0.09	0.09 ± 0.05	0.998 ± 0.002	0.1
HMDB00094	Citrate	12.5-100	0.59 ± 0.22	-0.43 ± 0.18	0.997 ± 0.004	0.5
HMDB01058	Fructose-1,6-diphosphate	3.125-50	0.32 ± 0.04	-2.27 ± 0.43	0.997 ± 0.002	0.02
HMDB00122	Glucose	25-200	0.002 ± 0.001	-0.010 ± 0.005	0.999 ± 0.0003	1.4
HMDB00148	Glutamate	1.25-20	0.25 ± 0.04	-1.10 ± 0.40	0.999 ± 0.001	0.09
HMDB00641	Glutamine	3.125-50	0.57 ± 0.14	1.72 ± 0.14	0.991 ± 0.005	0.2
HMDB03337	Glutathione (oxidized)	3.125-50	0.14 ± 0.01	-0.04 ± 0.01	0.994 ± 0.004	0.1
HMDB00125	Glutathione (reduced)	6.25-50	0.45 ± 0.17	-0.09 ± 0.01	0.991 ± 0.008	0.1
HMDB00139	Glycerate	1.25-20	0.07 ± 0.01	0.11 ± 0.02	0.995 ± 0.004	0.02
HMDB01397	GMP	12.5-100	0.04 ± 0.01	-0.98 ± 0.21	0.995 ± 0.002	0.4
HMDB01401/HMDB01586	Hexose 6-phosphate	6.25-100	0.05 ± 0.01	-2.31 ± 0.27	0.998 ± 0.001	1.9
HMDB00177	Histidine	2.5-40	1.12 ± 0.04	-1.08 ± 0.33	0.996 ± 0.002	0.6
HMDB00157	Hypoxanthine	6.25-100	3.64 ± 0.50	-2.58 ± 0.76	0.999 ± 0.001	0.02
HMDB00175	IMP	12.5-100	0.03 ± 0.01	-0.25 ± 0.12	0.999 ± 0.0001	0.1
HMDB00195	Inosine	0.12-2	4.80 ± 0.77	-0.65 ± 0.34	0.995 ± 0.004	0.01
HMDB00190	Lactate	125-2000	0.02 ± 0.005	1.65 ± 0.61	0.996 ± 0.002	10.2
HMDB00182	Lysine	2.5-40	0.10 ± 0.01	-0.02 ± 0.01	0.997 ± 0.001	0.1
HMDB00156	Malate	6.25-100	0.42 ± 0.10	1.89 ± 0.73	0.994 ± 0.007	1.3
HMDB01406	Nicotinamide	2.5-40	1.08 ± 0.16	-0.71 ± 0.07	0.996 ± 0.003	0.01
HMDB00159	Phenylalanine	2.5-40	0.86 ± 0.20	-0.56 ± 0.23	0.998 ± 0.001	0.1
HMDB01565	Phosphocholine	1.5-20	0.29 ± 0.06	-0.07 ± 0.02	0.999 ± 0.0003	0.45
HMDB00263	Phosphoenolpyruvate	6.25-50	0.01 ± 0.001	0.04 ± 0.01	0.995 ± 0.003	0.6
HMDB00939	SAH	0.625-10	0.90 ± 0.05	-0.36 ± 0.09	0.997 ± 0.002	0.02
HMDB14266	SAMe	0.625-10	0.18 ± 0.03	0.15 ± 0.07	0.994 ± 0.005	0.03
HMDB00187	Serine	1.25-20	0.21 ± 0.07	0.48 ± 0.13	0.992 ± 0.007	0.7
HMDB00251	Taurine	1.25-20	0.43 ± 0.19	0.29 ± 0.06	0.997 ± 0.003	0.03
HMDB00167	Threonine	2.5-40	0.59 ± 0.09	-0.15 ± 0.07	0.996 ± 0.005	0.2
HMDB30396	Tryptophan	2.25-20	0.06 ± 0.01	-0.20 ± 0.04	0.993 ± 0.002	0.1
HMDB00158	Tyrosine	2.5-20	0.62 ± 0.16	-1.17 ± 0.54	0.992 ± 0.003	0.3
HMDB00296	Uridine	1.25-10	0.53 ± 0.22	-0.31 ± 0.24	0.989 ± 0.011	0.2
HMDB00883	Valine	6.25-50	0.15 ± 0.04	-0.31 ± 0.29	0.991 ± 0.006	0.2
HMDB00292	Xanthine	0.3-5	2.67 ± 0.53	-0.75 ± 0.36	0.994 ± 0.005	0.02

Table S2. Quantitative analysis for selected extracellular metabolites (exometabolomics measurements).

HMDB ID	Metabolite	Linear range (mg/L)	Slope ± STD	Intercept ± STD	r ± STD	LLOD (mg/L)
HMDB00687/HMDB0000172	(Iso)leucine	3.75-60	0.08 ± 0.02	0.04 ± 0.02	0.998 ± 0.003	1.4
HMDB00267	5-oxoproline	10-160	0.50 ± 0.11	3.13 ± 0.57	0.986 ± 0.004	1.9
HMDB00958	Aconitate	1.25-20	1.18 ± 0.13	0.29 ± 0.06	0.992 ± 0.002	0.4
HMDB00034	Adenine	5-80	1.24 ± 0.15	-1.67 ± 0.14	0.999 ± 0.0001	0.04
HMDB00062	Carnitine	0.12-2	0.31 ± 0.01	-0.05 ± 0.01	0.999 ± 0.0001	0.06
HMDB00097	Choline	0.312-5	0.17 ± 0.04	0.20 ± 0.01	0.996 ± 0.002	0.1
HMDB00094	Citrate	12.5-100	0.19 ± 0.05	-1.13 ± 0.34	0.994 ± 0.004	0.5
HMDB00148	Glutamate	1.25-20	0.23 ± 0.01	-0.07 ± 0.02	0.999 ± 0.0003	0.09
HMDB00641	Glutamine	3.125-50	0.95 ± 0.13	-0.96 ± 0.11	0.994 ± 0.004	0.2
HMDB03337	Glutathione (oxidized)	3.125-50	0.28 ± 0.04	-0.28 ± 0.05	0.990 ± 0.002	0.1
HMDB00125	Glutathione (reduced)	6.25-50	0.11 ± 0.03	2.19 ± 0.7	0.985 ± 0.036	0.1
HMDB00139	Glycerate	1.25-20	0.05 ± 0.01	0.14 ± 0.03	0.986 ± 0.006	0.02
HMDB00177	Histidine	2.5-40	1.72 ± 0.39	-0.33 ± 0.10	0.999 ± 0.001	0.6
HMDB00157	Hypoxanthine	6.25-100	2.31 ± 0.33	2.09 ± 0.36	0.998 ± 0.002	0.02
HMDB00195	Inosine	0.12-2	6.13 ± 0.27	-0.34 ± 0.07	0.999 ± 0.001	0.01
HMDB00182	Lysine	2.5-40	0.19 ± 0.05	0.03 ± 0.02	0.999 ± 0.001	0.1
HMDB00156	Malate	6.25-100	0.27 ± 0.02	2.80 ± 0.39	0.991 ± 0.002	1.3
HMDB00765	Mannitol	625-5000	0.03 ± 0.01	-1.38 ± 0.60	0.999 ± 0.001	28.9
HMDB01406	Nicotinamide	2.5-40	0.29 ± 0.04	0.01 ± 0.01	0.996 ± 0.003	0.01
HMDB00159	Phenylalanine	2.5-40	0.85 ± 0.19	-0.46 ± 0.19	0.999 ± 0.0001	0.1
HMDB00187	Serine	1.25-20	0.12 ± 0.09	0.38 ± 0.27	0.997 ± 0.002	0.7
HMDB00296	Uridine	1.25-10	0.31 ± 0.21	-0.16 ± 0.17	0.995 ± 0.007	0.2
HMDB00292	Xanthine	0.3-5	1.18 ± 0.13	-0.67 ± 0.41	0.998 ± 0.003	0.02

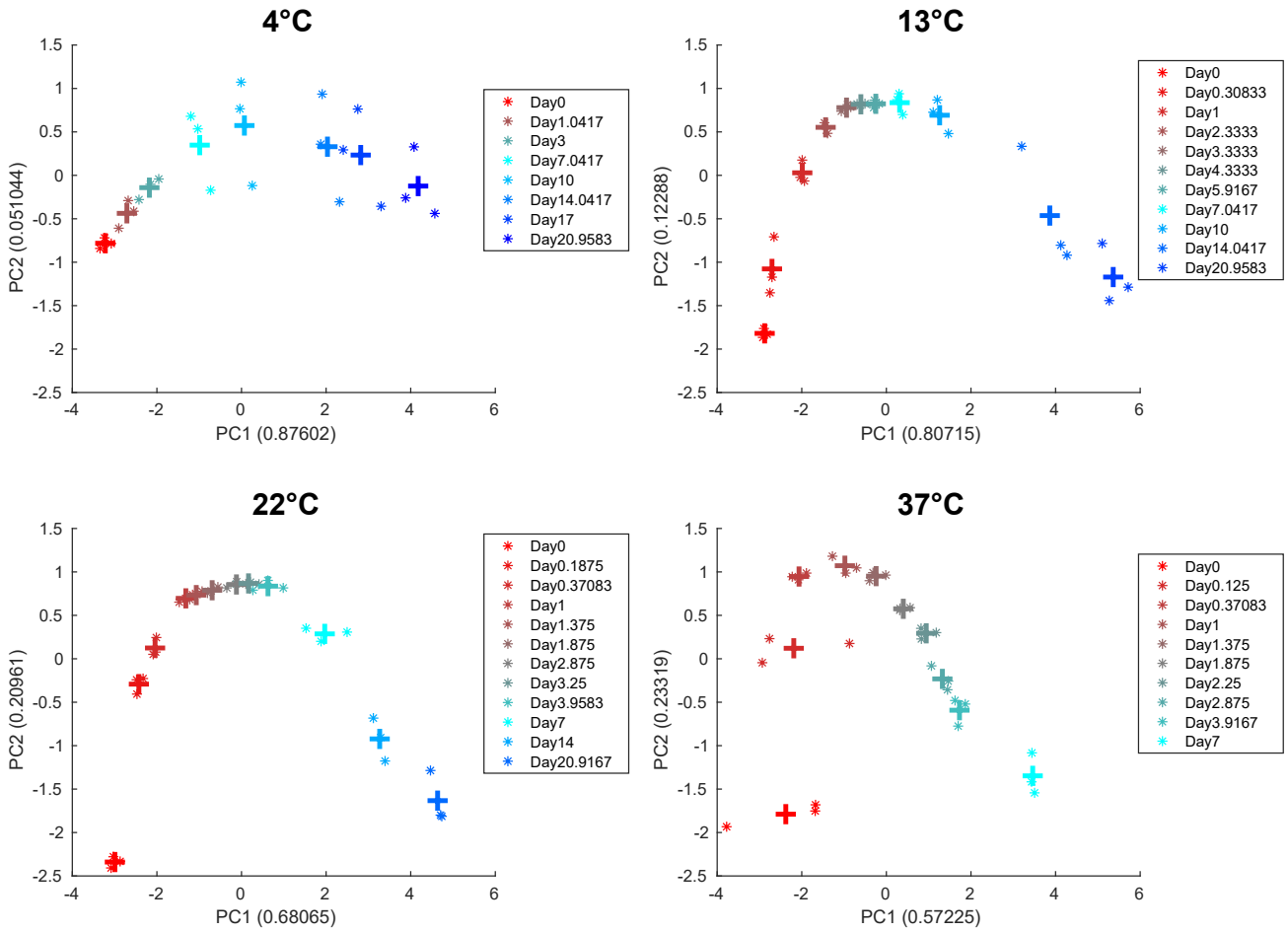

Fig. S1. Principal component analysis of the eight extracellular biomarkers. PCA of the 4°C data yielded loading coefficients that were then applied to the data at the other temperatures.

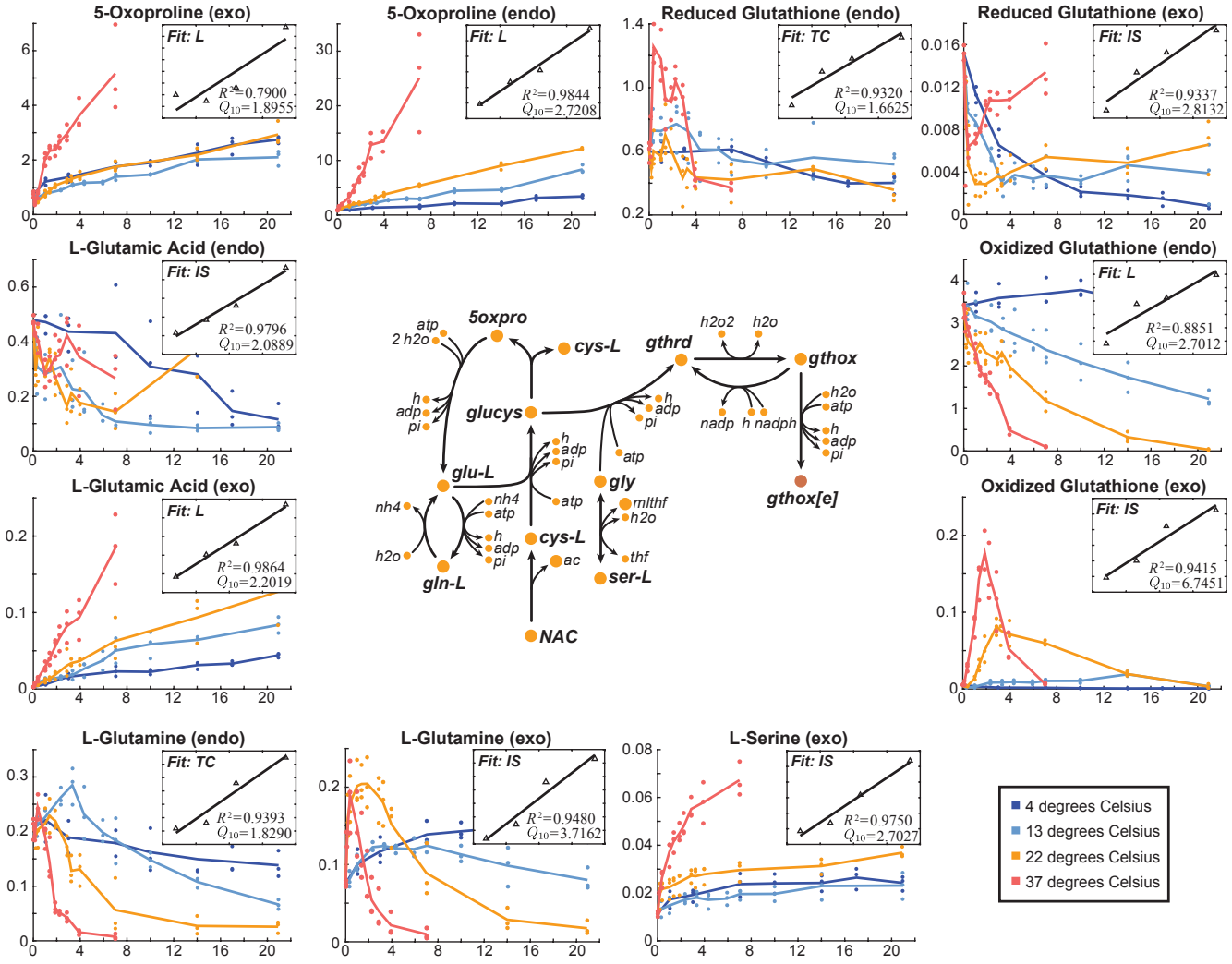

Fig. S2. Metabolic map of glutathione synthesis. The y-axis for metabolites is concentration (mM); the x-axis for metabolites is time (days). Day 0 here is taken to be 1 day after the beginning of the storage period. The y-axis for inset plots is $\log_2$(rate) where rate in units of concentration per time; the x-axis for inset plots is temperature (°C).

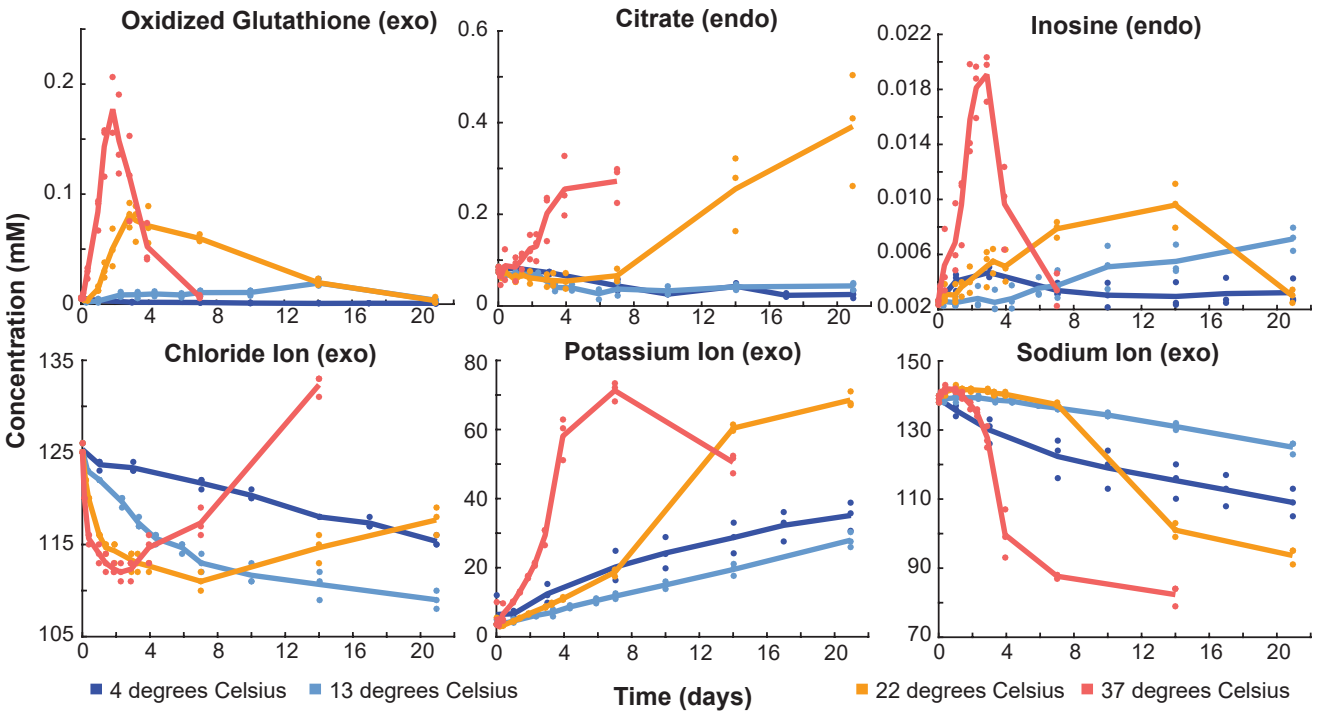

Fig. S3. Measurements with qualitative time course differences at higher temperatures and measured ions. Day 0 here is taken to be 1 day after the beginning of the storage period.

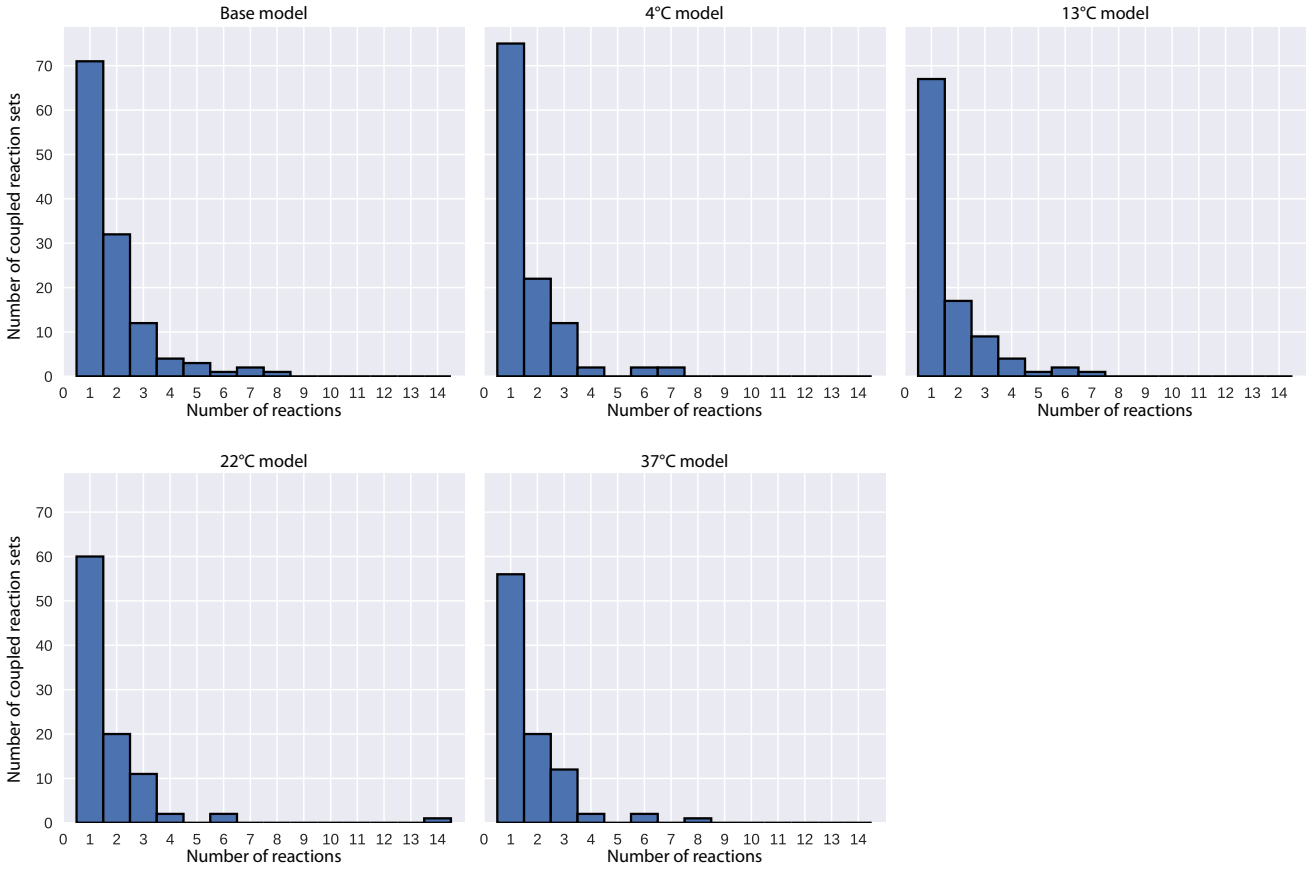

Fig. S4. Histograms of the number of coupled reaction sets separated by the number of reactions per set. The base RBC model is compared with the number of coupled reaction sets for each temperature's model.

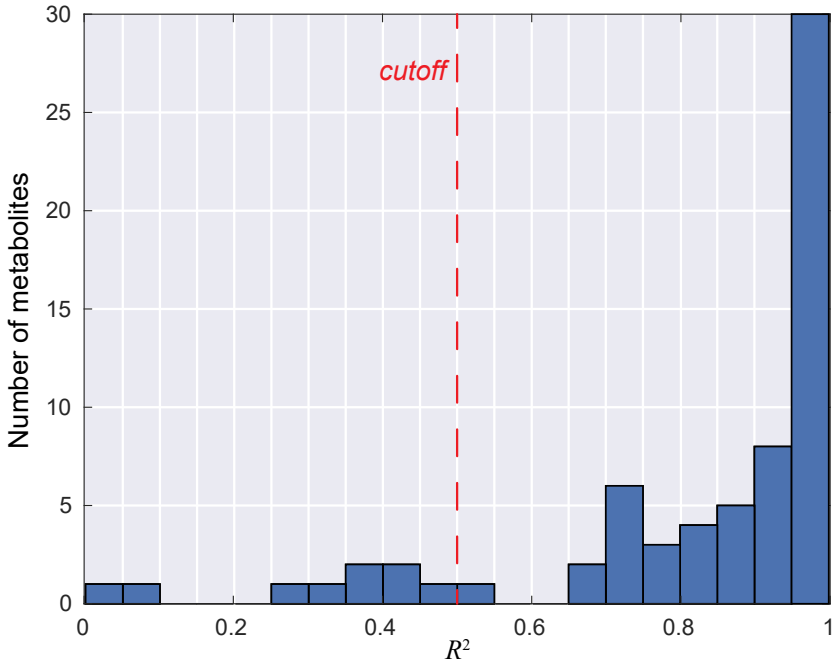

Fig. S5. Histogram of the the R^2 value for metabolites. The cutoff (at R^2 = 0.50) was used to exclude data that was poorly fit using linear regression.

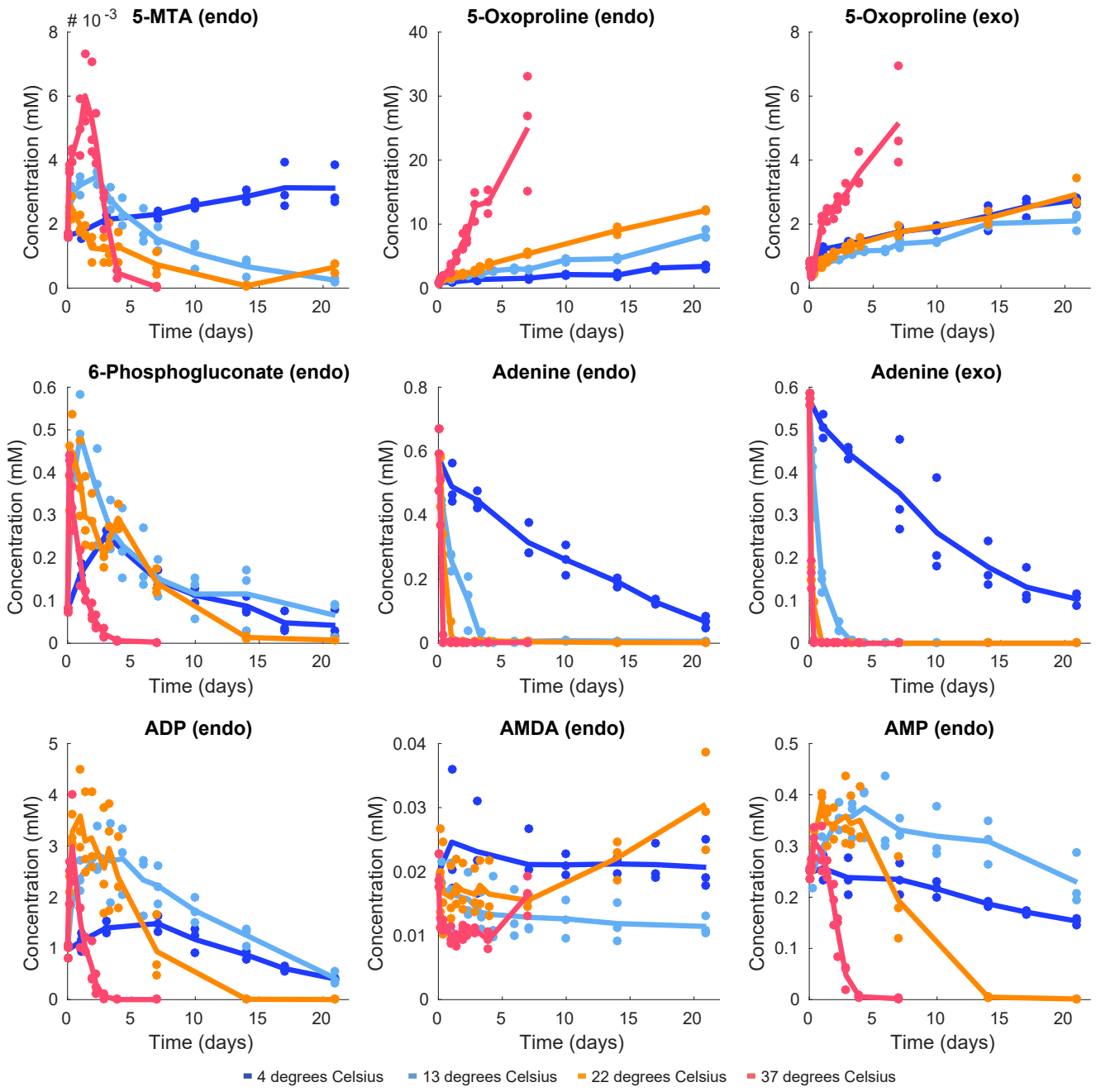

Fig. S6. Concentration vs time plots for all measurements.

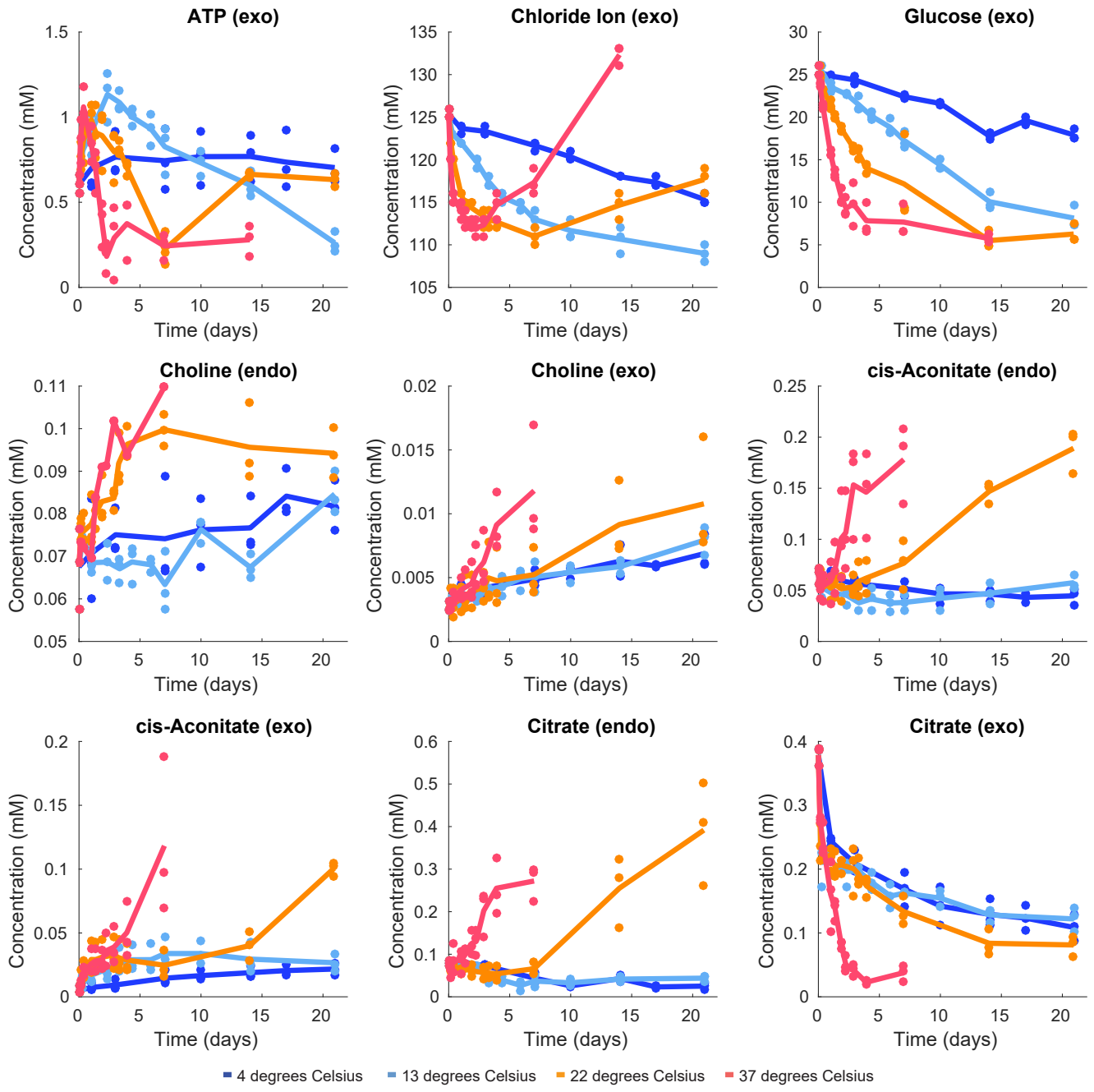

Fig. S7. Concentration vs time plots for all measurements.

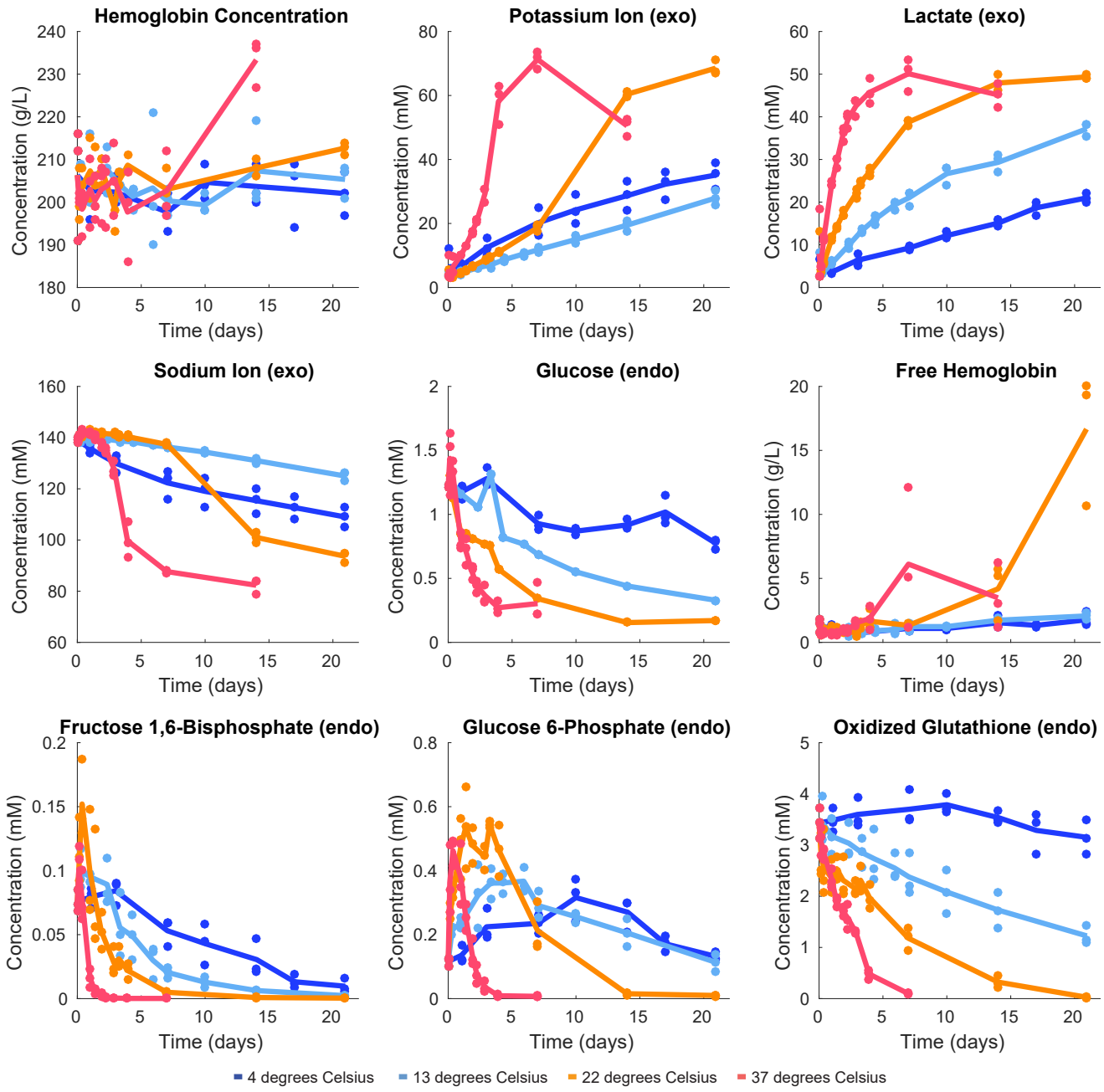

Fig. S8. Concentration vs time plots for all measurements.

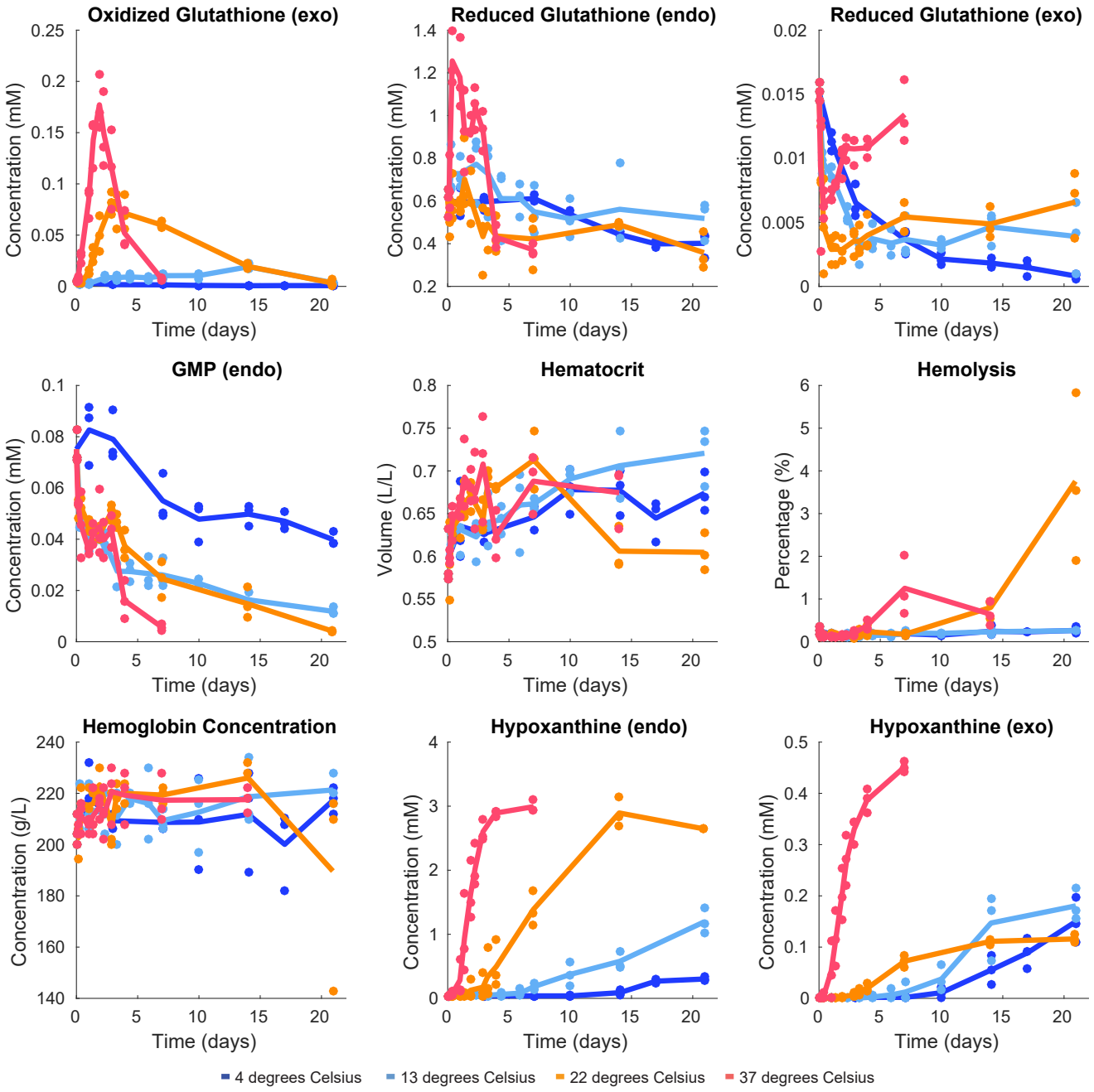

Fig. S9. Concentration vs time plots for all measurements.

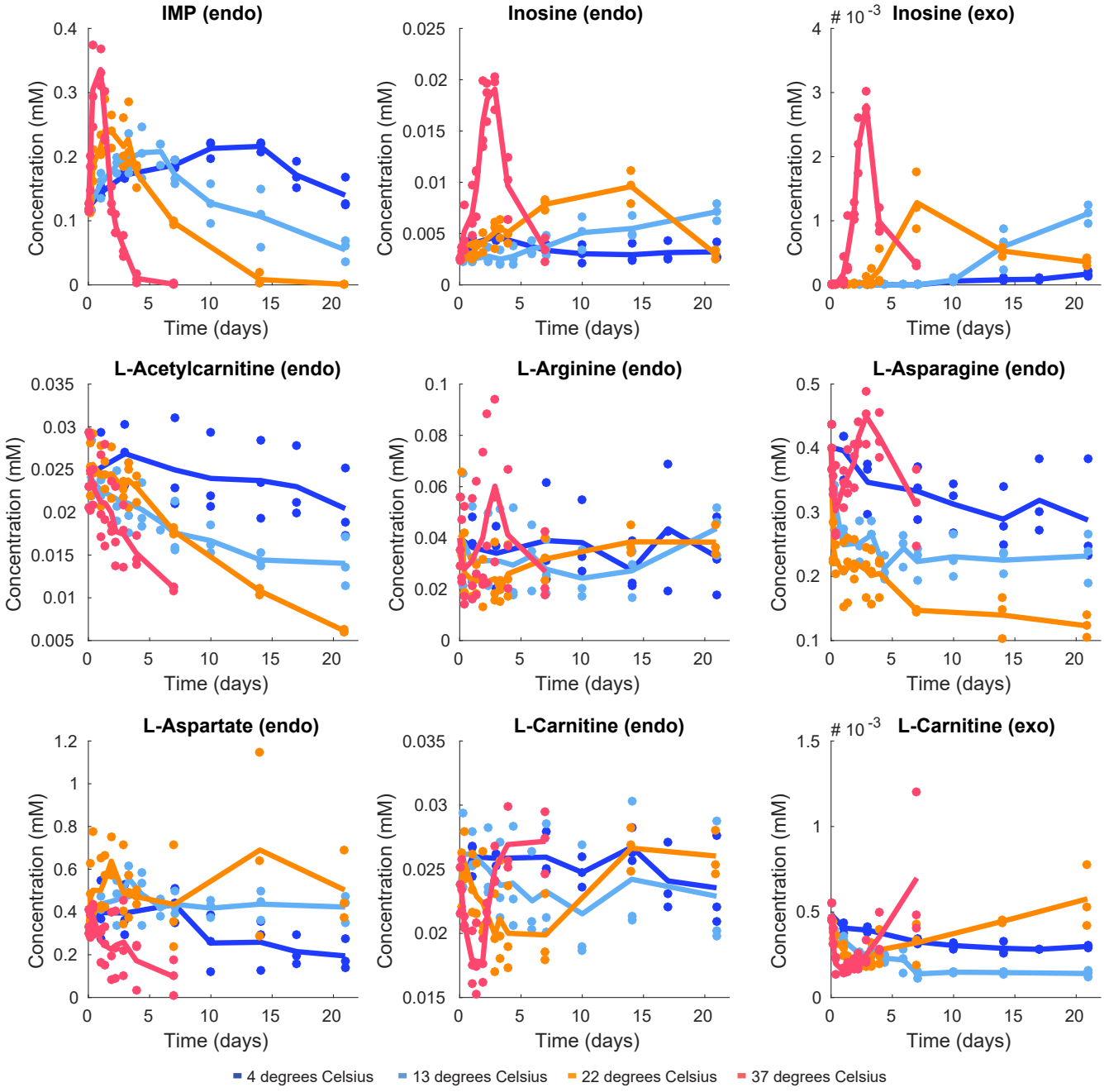

Fig. S10. Concentration vs time plots for all measurements.

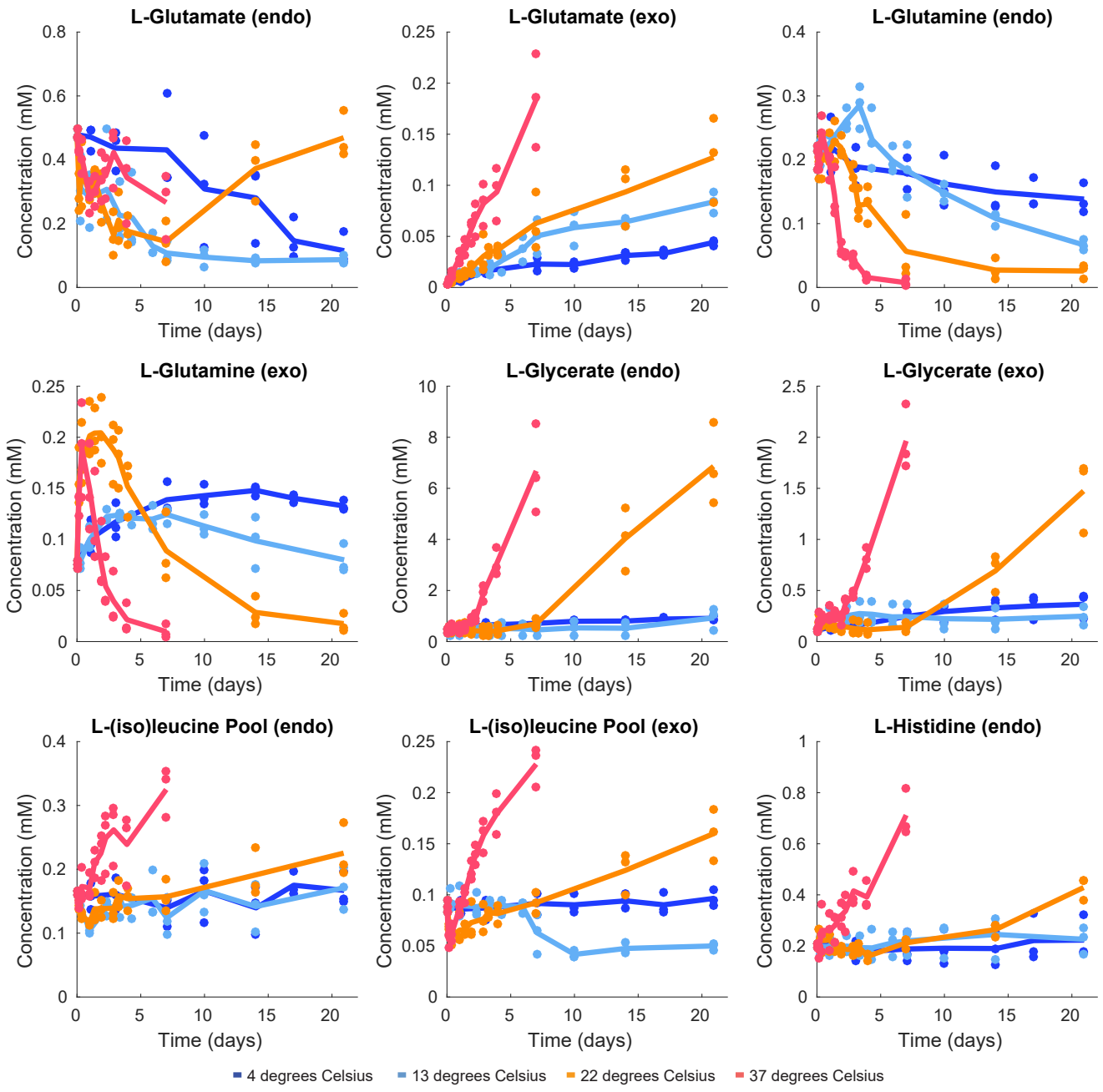

Fig. S11. Concentration vs time plots for all measurements.

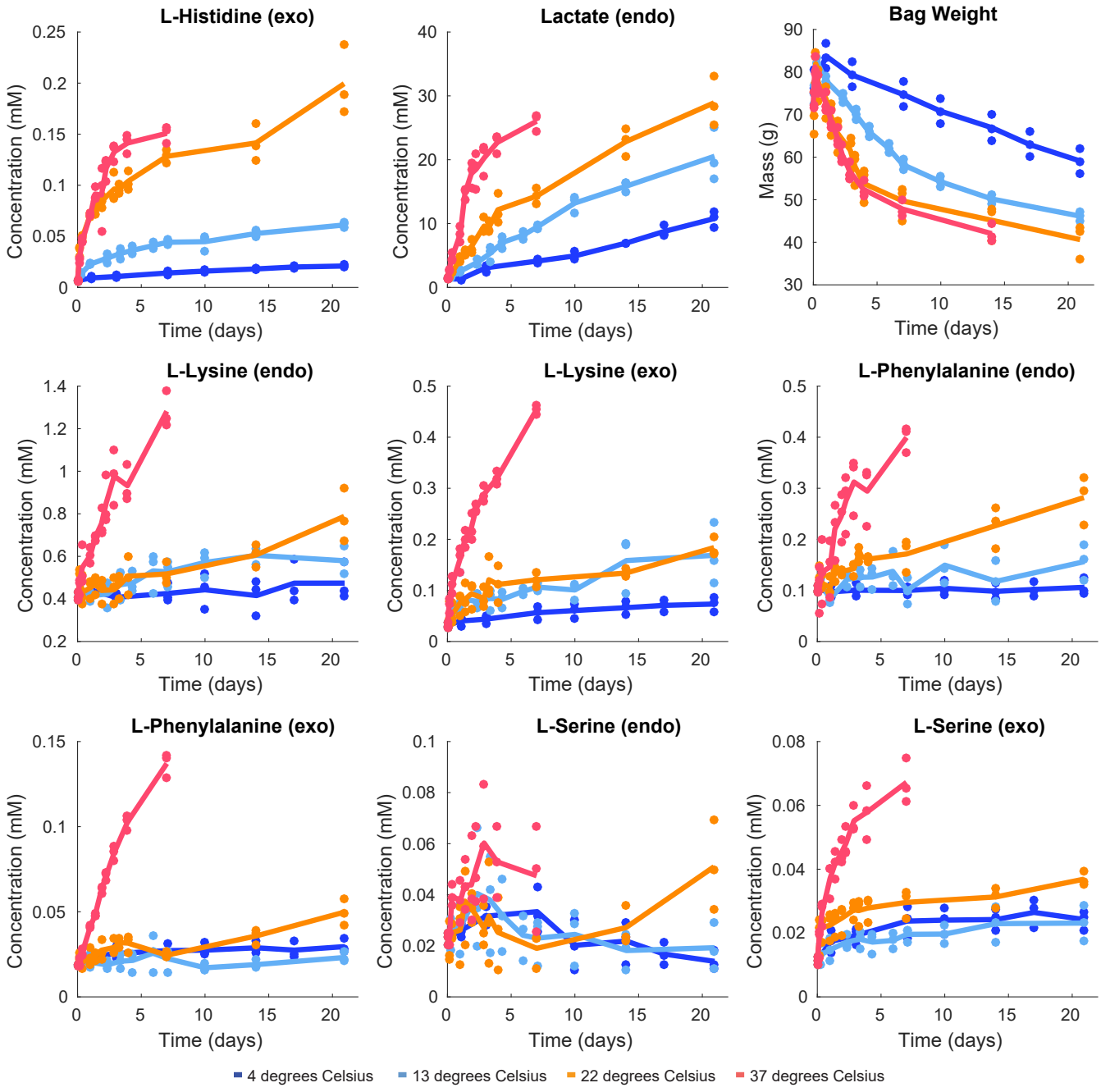

Fig. S12. Concentration vs time plots for all measurements.

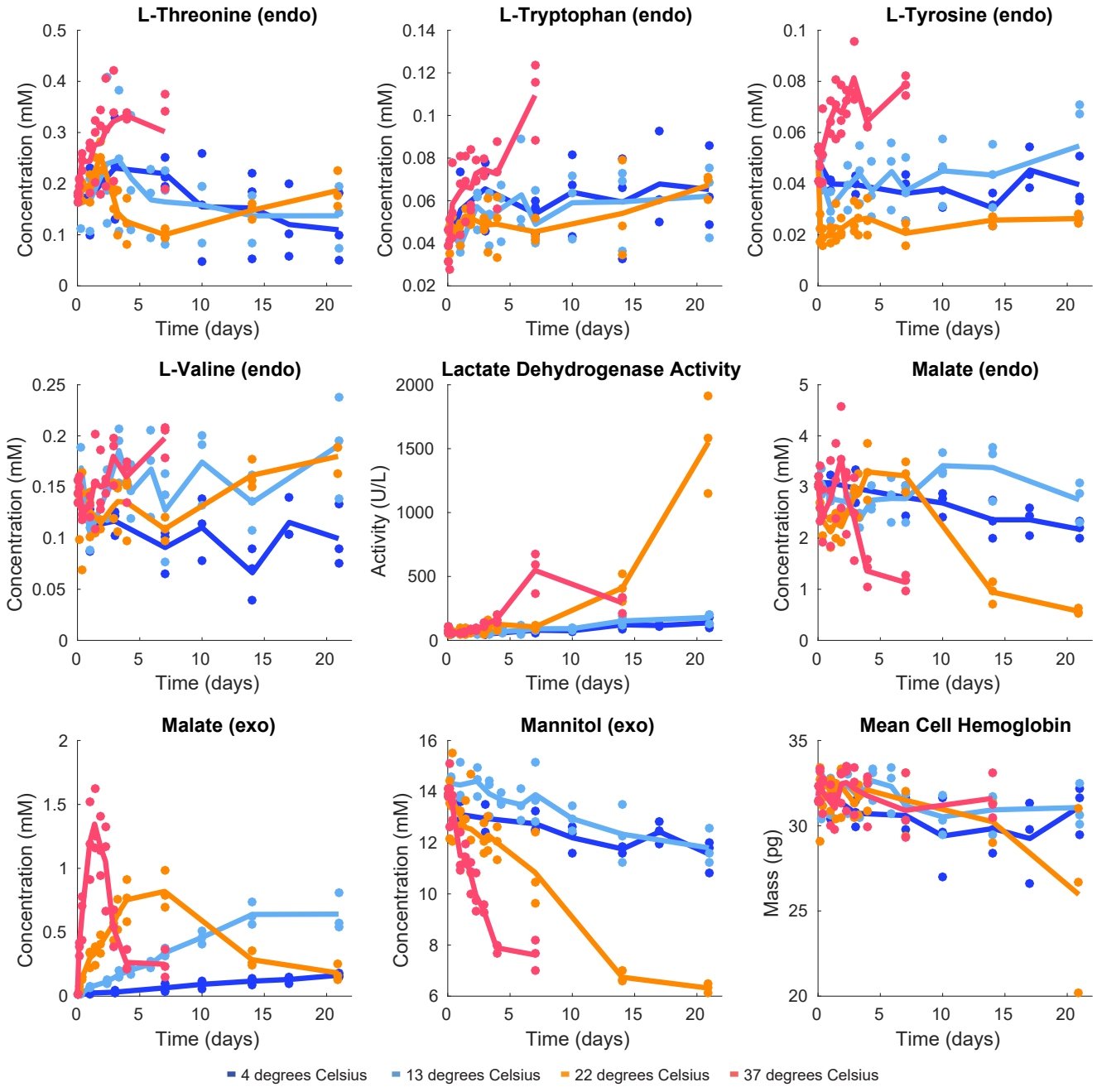

Fig. S13. Concentration vs time plots for all measurements.

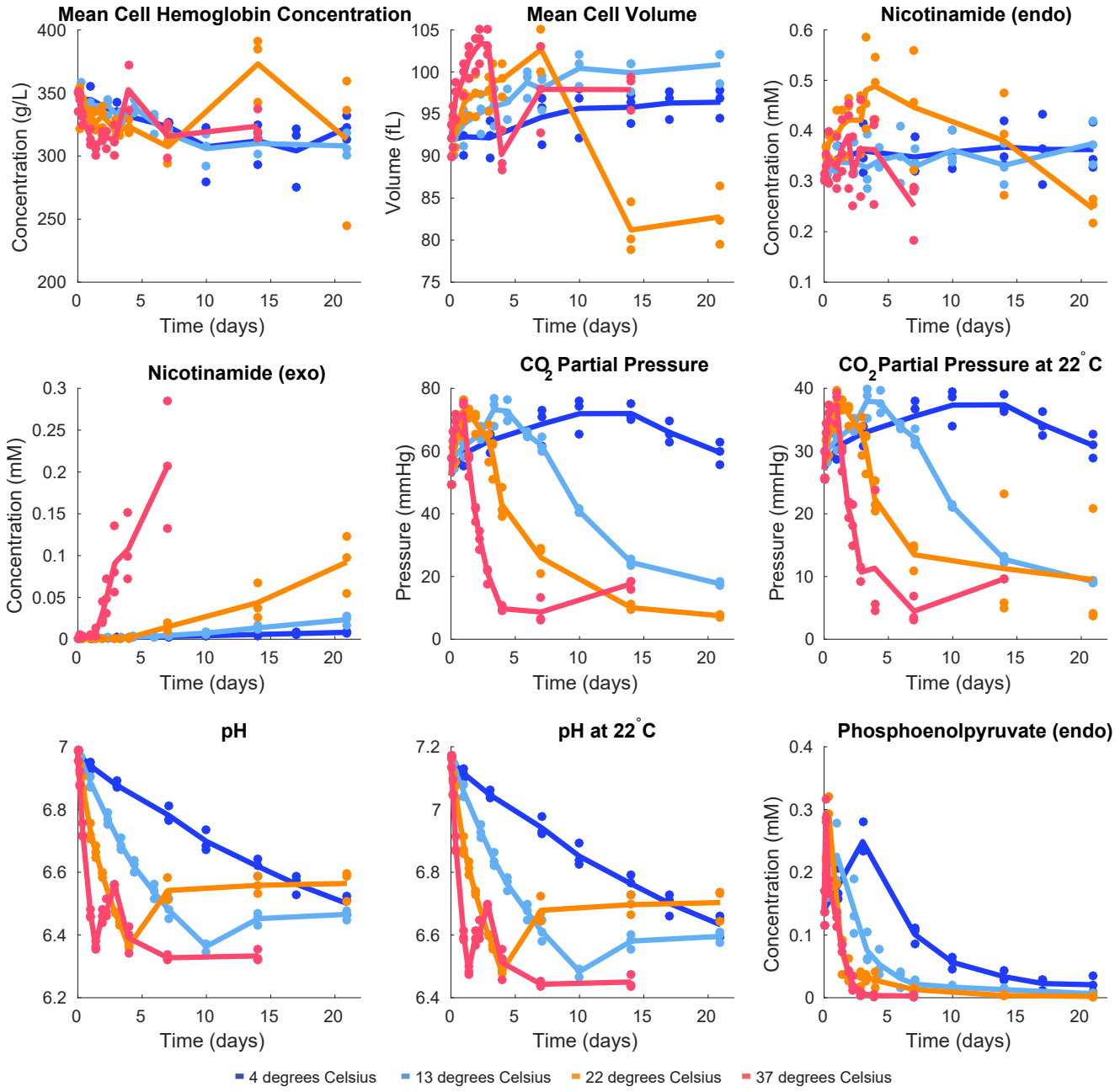

Fig. S14. Concentration vs time plots for all measurements.

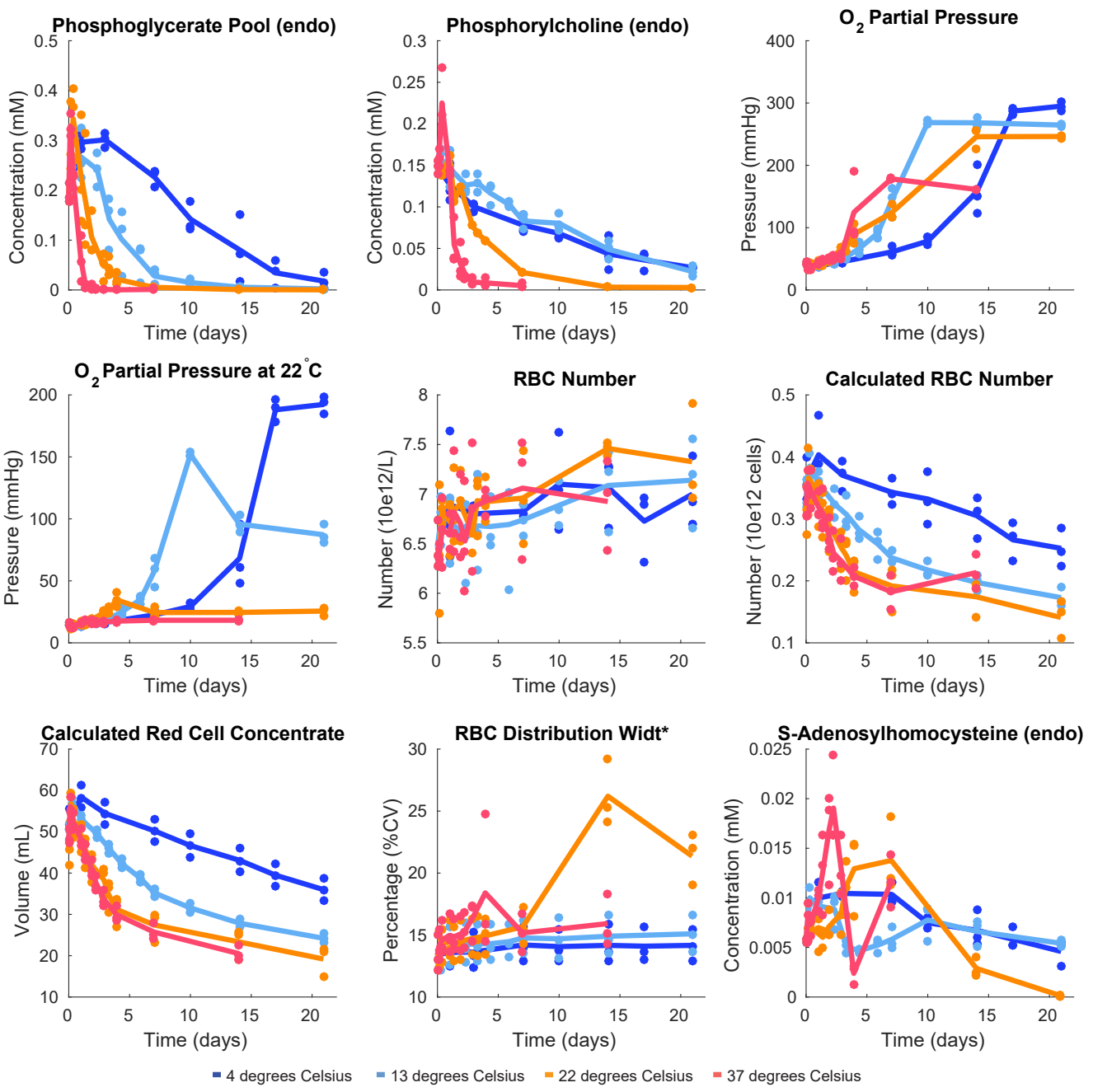

Fig. S15. Concentration vs time plots for all measurements.

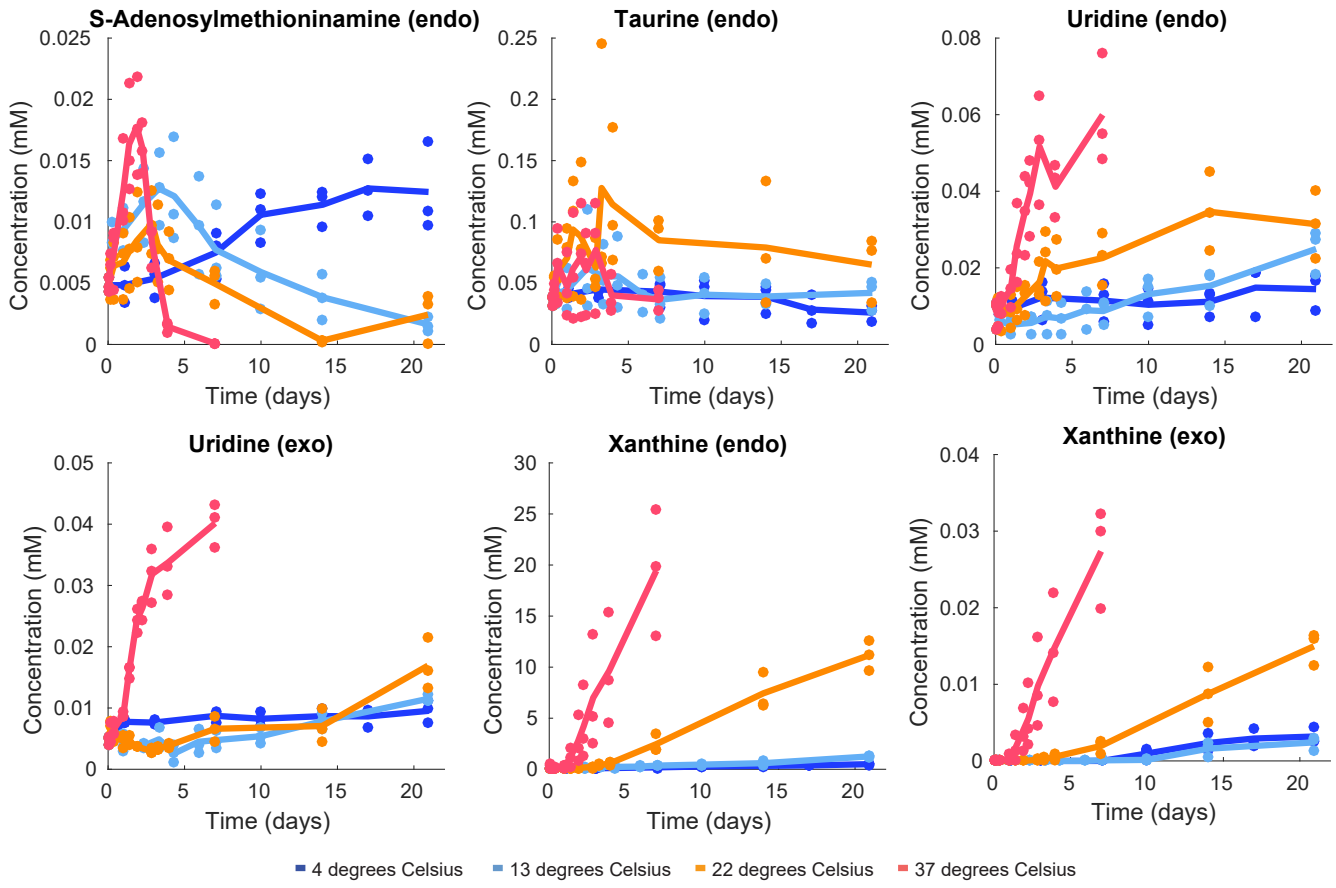

Fig. S16. Concentration vs time plots for all measurements.

References

1. D'Alessandro A, Liumbruno G, Grazzini G, Zolla L (2010) Red blood cell storage: the story so far. *Blood Transfus.* 8(2):82–88.
2. D'Alessandro A, et al. (2015) An update on red blood cell storage lesions, as gleaned through biochemistry and omics technologies. *Transfusion* 55(1):205–219.
   Bordbar A, et al. (2016) Identified metabolic signature for assessing red blood cell unit quality is associated with endothelial damage markers and clinical outcomes. *Transfusion* 56(4):852–862.
3. Wallas CH (1979) Sodium and potassium changes in blood bank stored human erythrocytes. *Transfusion* 19(2):210–215.
4. Högman CF, Meryman HT (1999) Storage parameters affecting red blood cell survival and function after transfusion. *Transfus. Med. Rev.* 13(4):275–296.
5. Hamasaki N, Yamamoto M (2000) Red blood cell function and blood storage. *Vox Sang.* 79(4):191–197.
6. Chang RL, et al. (2013) Structural systems biology evaluation of metabolic thermotolerance in escherichia coli. *Science* 340(6137):1220–1223.
7. Bordbar A, Jamshidi N, Palsson BO (2011) iAB-RBC-283: A proteomically derived knowledge-base of erythrocyte metabolism that can be used to simulate its physiological and patho-physiological states. *BMC Syst. Biol.* 5:110.
8. Bordbar A, et al. (2015) Personalized Whole-Cell kinetic models of metabolism for discovery in genomics and pharmacodynamics. *Cell Syst* 1(4):283–292.
9. Yurkovich JT, Yang L, Palsson BO (2017) Biomarkers are used to predict quantitative metabolite concentration profiles in human red blood cells. *PLOS Computational Biology*.
10. Larhlimi A, David L, Selbig J, Bockmayr A (2012) F2c2: a fast tool for the computation of flux coupling in genome-scale metabolic networks. *BMC Bioinformatics* 13(1):57.